NUCLEAR INSTRUMENTS AND METHODS 126 (1975) 205–215; © NORTH-HOLLAND PUBLISHING CO.

THE OPTIMIZATION OF A RUTHERFORD BACKSCATTERING GEOMETRY FOR ENHANCED DEPTH RESOLUTION

J. S. WILLIAMS

Department of Electrical Engineering, University of Salford, Salford M5 4WT, Lancashire, U.K.

Received 7 March 1975

A simple geometrical method for improving the depth resolution of the RBS technique is presented. A critical appraisal of the resolution-limiting factors such as beam collimation, detector acceptance angle, multiple scattering, and surface topography effects is given in an attempt to optimize the geometry for maximum attainable depth resolution. An optimized low-angle geometry in which the incident beam impinges onto the target surface at 5° and the detector is positioned for 168° scattering leads to ~8 times resolution improvement: the expected system depth resolution becomes 20–30 Å for a solid-state detector (15 keV fwhm). The effects of multiple scattering and surface topography on system resolution are examined experimentally: for carefully prepared target surfaces (vibratory polished and etched) system resolutions approaching those expected from the optimum RBS geometry can be attained in practice for near-surface analysis. At large analysis depths and for samples with ill-prepared surfaces the system resolution will be noticeably degraded and the resolution profile may become decidedly asymmetric.

I. Introduction

Over the past few years Rutherford backscattering (RBS) has been increasingly used as an analytical tool for studying the para-surface regions of solids[1,2]). By providing a measure of the elemental composition of thin films, it has met with success as a direct means for monitoring stoichiometry changes[3]) and detecting surface/bulk contaminants[4]). Furthermore, by providing depth analysis RBS has prompted recent applications to the study of interdiffusion of solid films[5,6]). However, the advent of ion implantation in many diverse fields, as a convenient means of introducing foreign impurities into the surface layers of a solid, has stimulated the major interest in the backscattering technique. For example, RBS has been used extensively both for direct monitoring of the accumulation of implanted species[7,8]) and, when used in conjunction with the channelling technique, for providing a measure of the ion damage and foreign atom location within the substrate[9,10]). More recent metallurgical and materials science applications of high dose implantation, for forming test alloys with superior chemical and physical properties[11–13]), have necessitated measurement of high-concentration impurity profiles. In such cases, the standard stripping techniques may not provide a reliable profile measurement[14]) and Rutherford backscattering thus presents itself as a desirable alternative mode of analysis.

The main limitations of Rutherford backscattering are:

(1) that analysis is often restricted to systems with heavy impurity atoms and light target atoms;
(2) that the measured backscattered signal is averaged over the entire irradiated area; and
(3) that the detector resolution usually limits the depth resolution to a few hundred Ångstroms.

The first limitation can be partly overcome by using thin targets[15]), employing channelling[16]) or using an appropriate nuclear reaction[17]), but even so the "background" will be high, making quantitative analysis difficult. As a result of limitation (2), the presence of localised, structural features in the composite target, such as precipitation effects, are not readily identified from backscattering data alone and some complementary means of analysis (e.g. TEM, X-ray diffraction) should be employed. Combined RBS and TEM studies have already met with considerable success in the analysis of high dose implantations[18,19]). High depth resolution is a necessary requirement in most of the RBS applications mentioned above, since the region of prime interest in interdiffusion and high dose implantation studies is frequently at, or in close proximity to, the film interface or target surface. However, the RBS depth resolution is often insufficient for probing these interesting surface regions on a small enough scale and unusual behaviour may go unresolved[20]). Rubin[21]), in the original treatise on Rutherford backscattering as an analytical tool, appreciated this problem and pointed out that both the energy resolution of the detection system and the system geometry were important factors determining

the available depth resolution. Since then, improvement of the detector energy resolution has been the major practical concern[22,23]), and the simpler approach, changing the system geometry, until now has received only limited attention in the literature[23-27]).

In a recent communication[28]) it was demonstrated how careful optimization of backscattering geometry can lead to better than a factor of 5 enhancement in depth resolution. The aim of this paper is to provide a more rigorous account of the technique and the considerations governing the optimum system geometry for maximum depth resolution. A critical appraisal of the limitations inherent in the method is also presented. The technique is illustrated with data from ion-implanted targets: in favourable circumstances, a depth resolution of up to 8 times that obtained with normal incidence geometries can be attained.

2. Basic considerations

2.1. Principles of geometrical resolution enhancement

A schematic of the backscattering arrangement indicating the relevant parameters is shown in fig. 1. For a probe beam of light ions (mass M_1, energy E_1) incident at an angle ϕ to the surface normal of a solid target (mass M_2), the energy of the exit beam E_b, backscattered through an angle $180^\circ - \theta$ is given by:

$$E_b = k^2(E_1 - \Delta E_{in}) - \Delta E_{out}. \quad (1)$$

Here:

$$k = (M_2 - M_1 \cos\theta)/(M_1 + M_2),$$

for $M_1 \ll M_2$, and ΔE_{in} and ΔE_{out} are the energy-loss components for the probe beam on the incident and exit paths, respectively. For shallow scattering depths, z, normal to the surface, the stopping power of the target for the probe beam (defined as the rate of change of energy with penetration depth) can be considered constant over the incident and exit paths. Eq. (1) may then be written in the form:

$$E_b = k^2\{E_1 - S_{in}(E)\, z/\cos\phi\} - S_{out}(E)\, z/\cos(\phi - \theta), \quad (2)$$

where S_{in} and S_{out} are the stopping-power components corresponding to ΔE_{in} and ΔE_{out}.

Data from RBS analyses are usually obtained in the form of energy spectra of backscattered particles. Using eq. (2), it is possible to relate a particular backscattered energy E_b to scattering from a unique depth z. The depth resolution of the detection system dz can be expressed in terms of the system energy resolution ΔE by differentiation of eq. (2) to yield:

$$dz = \Delta E/\{k^2 S_{in}(E)/\cos\phi + S_{out}(E)/\cos(\phi - \theta)\}. \quad (3)$$

An examination of eq. (3) suggests two possibilities for obtaining increased depth resolution:

(1) improving the energy resolution of the detection system; or

(2) employing a backscattering geometry with ϕ and $\phi - \theta$ large.

Improvement of the energy resolution of a solid-state detection system by using cooled detectors and preamplifiers and by optimization of associated electronics provides for an ultimate depth resolution of ~ 200 Å. The use of more complex detection systems with high energy resolution offers a better improvement in depth resolution, approaching the 20 Å resolution provided by a magnetic spectrometer[22]).

The geometrical enhancement in depth resolution is illustrated diagrammatically in fig. 2. Consider a uniform implanted layer of heavy ions 300–400 Å below the surface of a light substrate (e.g. Pb^+ implanted into Si). In a normal-incidence backscattering geometry using, say, 2 MeV He^+, the resolution of a solid-state detection system would not permit the true profile of the implanted layer to be clearly resolved: the measured profile (as shown in fig. 2) would be severely modified by the Gaussian-shaped detector profile. The only way any quantitative information could be extracted from such an energy spectrum is by

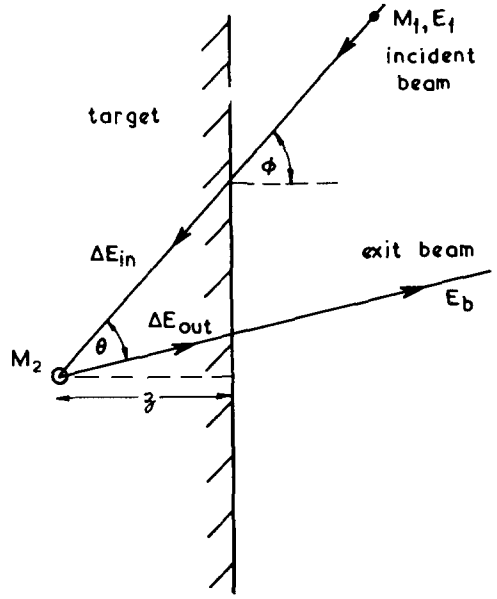

Fig. 1. A schematic of the RBS arrangement showing the relevant parameters (see text).

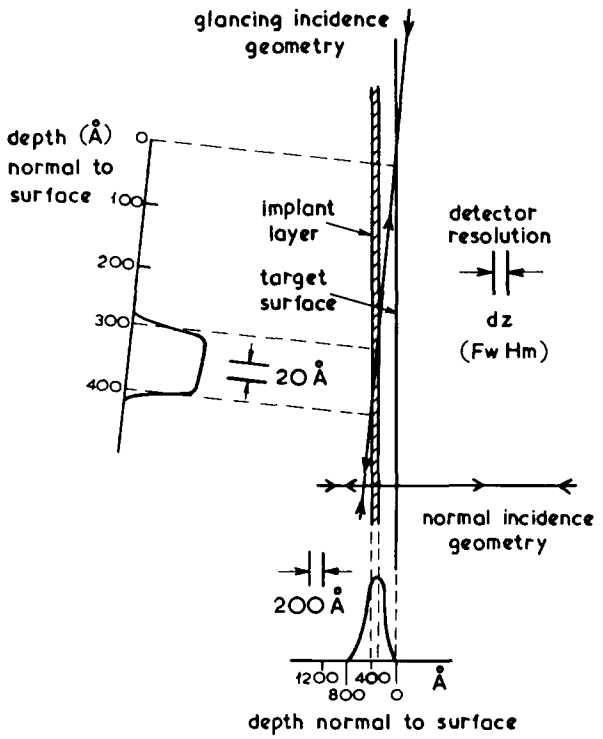

Fig. 2. Schematic illustration of the enhancement in depth resolution normal to the surface obtained with a glancing-angle RBS geometry. Normal-incidence and glancing-angle spectra are shown for backscattering from a uniform implant layer 100 Å wide and 400 Å below the target surface. The depth resolution is ~200 Å with normal incidence, and ~20 Å with the low-angle arrangement.

employing complicated deconvolution techniques[29, 30]), but this is valid only when the energy width of the signal from the implant layer is significantly greater than the detector energy resolution. Alternatively, if we employ a glancing-incidence geometry, as shown in the upper part of fig. 2 ($\phi \approx 84°$ and $\theta = 0°$) the path length of the probe beam in traversing the implanted layer is substantially increased. As a result, the energy difference between ions scattered from the front and back of the implanted layer is now much larger than the detector energy resolution and, consequently, a well-resolved profile of the implanted layer is obtained in the energy spectrum. With the glancing incidence geometry of fig. 2, the depth resolution normal to the target surface has been improved approximately 10 times – typically from 200 Å (normal incidence) to 20 Å.

Returning to eq. (3), it may seem that the depth resolution could be improved without bound, simply by choosing incident and exit paths inclined at smaller and smaller angles to the target surface. However, target flatness, surface roughness, beam collimation, detector acceptance angle, and multiple scattering of the probe beam are practical limitations to the attainable depth resolution. In the next section these shall be examined in detail in an attempt to optimize the backscattering geometry for maximum depth resolution.

2.2. Practical limits to depth resolution

The ultimate depth resolution of a particular Rutherford backscattering geometry, dz_T, can be expressed in terms of the expected depth resolution given by eq. (3), dz_G, and the uncertainty in scattering depth introduced by beam divergence, etc., dz_L:

$$dz_T = dz_G + dz_L . \tag{4}$$

The influence of the system geometry on the relative

Table I

A summary of the contribution to the resolution-limiting term dz_L.

Contribution	Origin	Comments
dz_E	Poor beam collimation	Not a problem
Inherent in the experimental arrangement	Finite detector acceptance angle	Restricts the position of the detector and the ultimate system resolution
dz_B	Multiple scattering from target atoms	Difficult to estimate; increases with depth; confines the analysis to the near-surface
Bulk target effects	Energy straggling process	Small contribution compared with multiple scattering
dz_S	Long-range surface flatness	Scale can be measured and dz_S estimated
Surface topography effects	Short-range surface roughness	Difficult to estimate and experimental characterisation a possible approach

magnitude of the limiting term dz_L, is best illustrated by an example. Consider an arrangement in which a 2 MeV He^+ beam is scattered from a Si target through 180° ($\theta = 0°$) into a solid-state detector with an energy resolution of 15 keV (fwhm). From eq. (3) the expected system depth resolution in normal incidence ($\phi = 0°$) and glancing incidence, say $\phi = 84°$, would be about 250 Å and 25 Å, respectively. If we now have an effective angular spread in both the incident and scattered beam of 1° (half angle) then, for scattering from 400 Å below the target surface, the uncertainty in depth arising from beam divergence alone can be estimated from eq. (3) as $dz_L \ll 10$ Å $\ll dz_G$ for normal incidence, and $dz_L \approx 60$ Å $> dz_G$ for glancing incidence. Hence, when low-angle RBS geometries are employed, all factors, such as beam divergence, which may contribute to dz_L and limit the attainable depth resolution must be carefully considered.

The term dz_L may be divided into three main contributions which can be conveniently treated separately and are summarised in table 1. The contribution dz_E, which arises from the fixed beam divergence inherent in the *experimental* arrangement as incident beam spread and detector acceptance angle, can be minimized by careful optimization of the experimental conditions. This is discussed in detail in section 2.3: suffice it to say here that careful choice of the experimental geometry can keep $dz_E \ll dz_G$ and at the same time provide a depth resolution enhancement of up to 10 times that obtained with normal-incidence geometries. The term dz_B which arises from small-angle (multiple) scattering of the probe ion from target atoms and energy straggling effects within the *bulk* target will increase in magnitude with path length. It is difficult to obtain a reliable estimate of dz_B as a function of depth, since multiple-scattering processes are not fully understood and the theoretical analysis is complex[31–33]). However, by confining the RBS analysis to the near-surface region of the target, the effective contribution of dz_B to the overall resolution can be minimized. The third contribution arising from *surface* irregularities, dz_S, can be subdivided further into long-range surface flatness effects which introduce an uncertainty into the angle of incidence of the probe beam, and localised short-range surface roughness (a series of "hills and valleys" maybe 10's or 100's of Ångstroms high and separated by similar distances) which presumably could introduce an uncertainty into the determination of the true position of the surface. The scale of long-range surface flatness is not difficult to measure (e.g. by optical interference methods), enabling the contribution to dz_S to be readily estimated for a particular scattering geometry. However, the effects of localized surface roughness on the system depth resolution are more difficult to predict, especially without a precise knowledge of the small-scale surface topography. An attempt has been made to experimentally estimate the contributions of dz_B and dz_S to the overall RBS depth resolution. The results are presented and discussed in section 3.

2.3. Optimization of the backscattering geometry

The main consideration in attempting to optimize the scattering geometry for maximum depth resolution is to

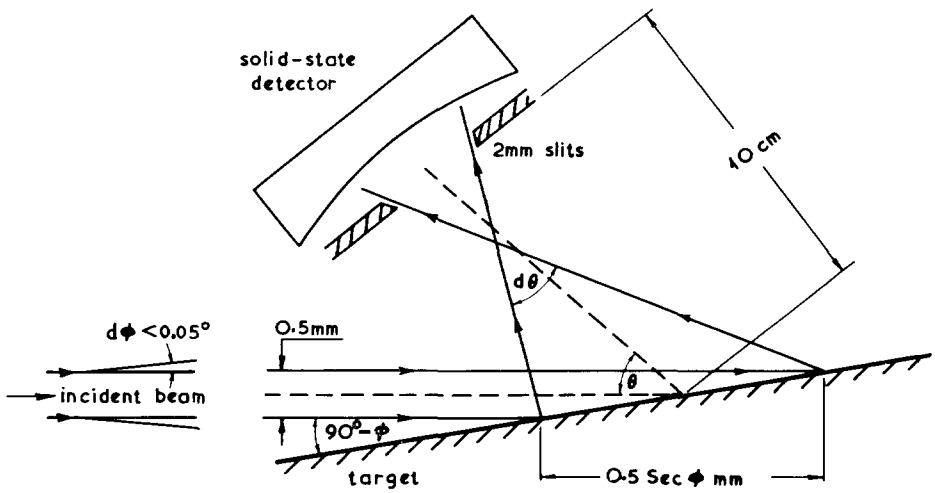

Fig. 3. The low-angle RBS geometry, showing the incident beam, angular divergence $d\phi$, impinging at an angle $90-\phi$ onto the target surface and scattered through an angle $180-\theta$ into a solid-state detector, acceptance angle (in the plane of the figure) of $d\theta$. Note the increased irradiated area with the low-angle geometry.

keep the contributions to dz_E small compared with our expected resolution dz_G. A schematic of the scattering geometry is shown in fig. 3, where the prime factors giving rise to dz_E are depicted; namely, incident beam divergence, $d\phi$, and detector acceptance angle, $d\theta$. Without any consideration for detection count rate it is possible, by suitable collimation of both the incident and scattered beams, to keep $dz_E \ll dz_G$ for practically any desired scattering geometry. However, the realistic detection count rates which must be employed in the interests of keeping both analysis time and probe beam flux to a minimum, will certainly influence $d\phi$ and $d\theta$. An additional, important consideration is that for low-angle-scattering geometries only the component of incident-beam divergence (lateral spread) in the plane of incidence will contribute significantly to dz_E. For simplicity, if the detector is also positioned in the incident plane, as shown in fig. 3, then the component of detector acceptance angle in the plane of incidence will similarly provide the major contribution to loss of depth resolution. Consequently, the detection count rate can to some extent be improved without a corresponding loss of depth resolution by employing a more diffuse probe beam and a larger detector acceptance angle in the plane *normal* to the plane of incidence.

In our experimental arrangement the incident beam has a cross section of 0.5×2 mm^2, the smaller dimension corresponding to a beam divergence of $d\phi \sim 0.05°$ in the plane of incidence (horizontal plane in our case). The physical dimensions of the scattering chamber and the conditions necessary for a suitable detection count rate have led to a 100 mm^2 detector being placed ~ 10 cm from the target (with 2 mm entrance slits to reduce the acceptance angle in the horizontal plane). Noting that the irradiated target area is greatly enlarged in low-angle geometries (by a factor sec ϕ as indicated in fig. 3), the detector acceptance angle in the horizontal plane, $d\theta$, for our arrangement will be $\sim 2°$–$3°$.

Knowing $d\phi$ and $d\theta$, the optimum backscattering geometry was obtained as follows. Firstly, with $d\phi \sim 0.05°$ and considering that the target surface should be capable of preparation to flatter than 0.1° over the irradiated area (e.g., by precision vibratory polishing conditions), the contribution to dz_E over the incident path length will be much smaller than dz_G (e.g. 5% in practice) if ϕ is less than about 85°. Similarly, with a detector acceptance angle $d\theta \sim 3°$, the scattering angle θ must be greater than about 12° in order to keep $dz_E \ll dz_G$. Hence, in our experimental arrangement the optimum geometry for maximum depth resolution would seem to be $\phi \approx 85°$ and $\theta \approx 12°$. Consequently, for a detector energy resolution of 15 keV fwhm, the maximum expected depth resolution would be of the order of 30 Å (using for example a 2 MeV He^+ probe incident on a Si target).

3. Experimental, results and discussion

3.1. Backscattering arrangement

The experimental RBS arrangement is shown schematically in fig. 4. The target is mounted on a 3-axis goniometer in an inclined holder to allow the incident beam to make a grazing angle with the target surface without striking the goniometer mechanism. A negative potential of 800 V applied to a copper ring incorporated into the target holder provides secondary-electron suppression, enabling the absolute beam current to be measured directly on target. Accurate alignment of the target surface to better than 0.05° with respect to the incident beam is achieved with the aid of a He–Ne laser pre-aligned co-linear with the analysing beam[34]). The ϕ and γ axes are first adjusted until both the incident laser beam and that reflected from the

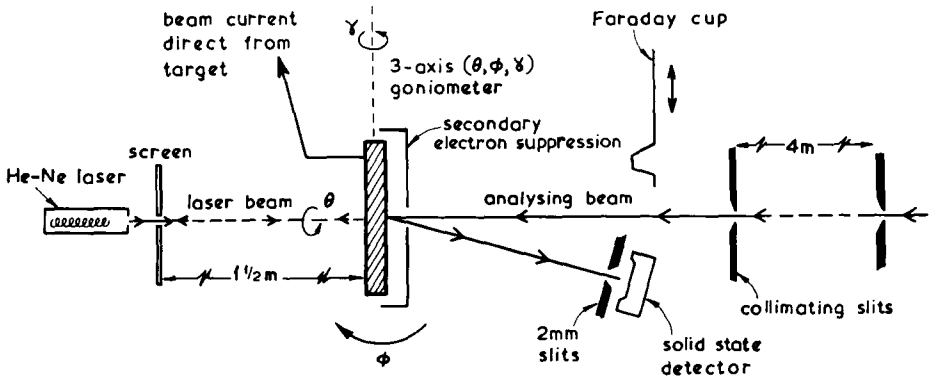

Fig. 4. The experimental arrangement showing the laser pre-alignment of the target and the He^+ analysis system.

target surface are aligned, then the ϕ axis is rotated 180° to achieve alignment of the target surface with the incident particle beam.

3.2. Demonstration of the technique

As a demonstration of the glancing-angle backscattering technique, a commercially prepared ⟨111⟩ Si wafer* was first implanted off-axis with 38 keV Pb^+ ions to a total dose of 5×10^{15} cm^{-2}, and then a trace amount of Au evaporated onto the surface. The sample was then analysed with 2 MeV He^+ ions using various backscattering geometries. Typical spectra are shown in fig. 5.

For implant energies less than about 50 keV, the depth resolution of the normal-incidence RBS system would not be sufficient to resolve the implant profile from a similar mass impurity at the target surface. This is seen in the spectrum of fig. 5(a), where the backscattered yield from both the Pb implanted atoms and the surface Au atoms appear as a single, unresolved peak. However, the spectra in figs. 5(b) and 5(c) clearly exhibit a marked improvement in the depth resolution of the backscattering system: with $\phi = 77°$ the Pb and Au peaks are just resolvable and with $\phi = 85°$ the resolution is further enhanced, clearly showing the shape of the Pb implant profile. In fig. 5, a resolution factor R – defined as the ratio of the normal-incidence depth resolution to that obtained with the low-angle geometry – has been used as a measure of the expected improvement in depth resolution in the spectra of (a), (b), and (c). For the geometry of fig. 5(c), the expected depth resolution [from eq. (3)] is ~ 40 Å and, when a depth scale is fitted to the spectrum [eq. (2)], the most probable range of the Pb-implanted profile can be estimated, from the position of the Pb peak, as ~ 250 Å. This value is in reasonable agreement with the range predicted on the basis of LSS theory (~ 205 Å) [35, 36].

An additional noteworthy feature evident in fig. 5 is the appearance of a dip (arrowed) in the Si substrate yield when glancing-angle geometries are employed. This effect can be explained in terms of the presence of a significant concentration of implanted species within the target, which results in an increased stopping power for the analysing beam[37]). Thus, the increased depth resolution of low-angle backscattering geometries can bring to light composite-target stopping-power effects not apparent in normal-incidence geometries.

* Mechanically and chemically polished by Dow Corning Co.

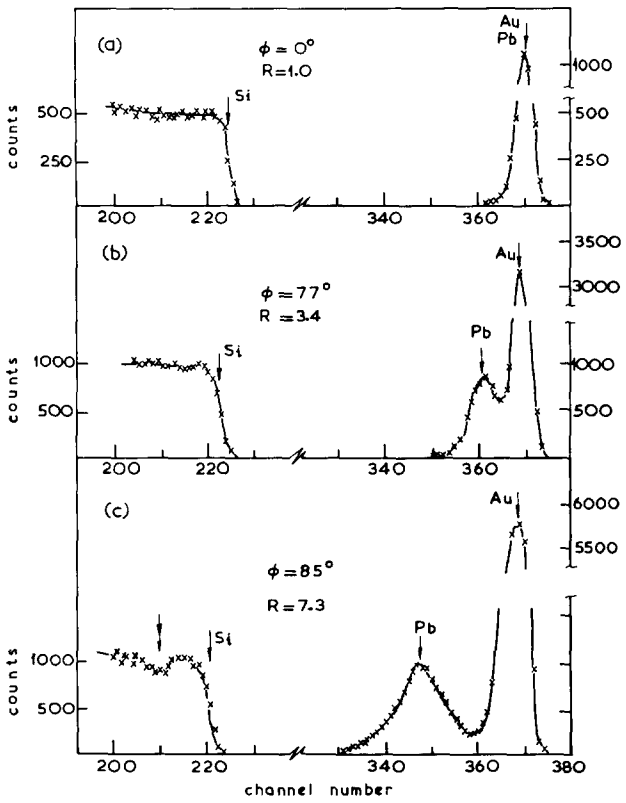

Fig. 5. 2 MeV He^+ backscattered spectra from a 38 keV Pb-implanted Si target with thin evaporated Au surface layer. Three scattering geometries are shown to illustrate the resolution enhancement at low-angle geometries; Pb dose 5×10^{15} cm^{-2}, 5 keV/channel.

3.3. Target surface and bulk effects on system resolution

To observe the effects of surface topography on RBS depth resolution "smooth" and "rough" Si

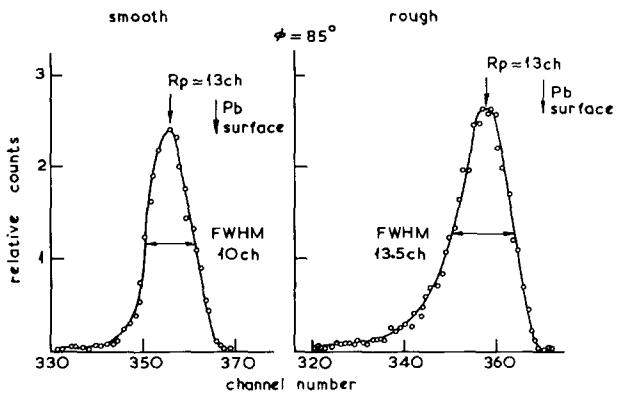

Fig. 6. 2 MeV He^+ spectra from 20 keV Pb^- ions implanted into "smooth" and "rough" Si targets at $\phi = 85°$ geometry; 5 keV/channel.

samples were simultaneously implanted with 20 keV Pb^+ ions to a dose of 10^{15} cm^{-2}. The "smooth" samples were carefully mechanically and chemically polished* and the "rough" samples were simply given a long chemical etch from a sawn surface. After implantation the samples were set up for $\phi = 85°$ glancing-angle RBS with 2 MeV He^+ ions. The "rough" samples were difficult to laser-align owing to a large angular divergence ($\sim 2°$) in the surface-reflected laser beam. Typical Pb-implanted profiles from both "smooth" and "rough" samples are shown in fig. 6.

Whereas the "smooth"-sample profile is near-Gaussian in shape, the "rough"-sample profile exhibits a marked "tail" and is clearly broader (fwhm 13.5 channels compared with the "smooth"-profile fwhm 10 channels). The Pb peak position in both cases is 13 channels below the surface, corresponding to a most probable range of $\sim$ 190 Å for 20 keV Pb^+ in Si. The broader, "rough"-sample profile is indicative of an overall loss of system depth resolution, the asymmetry presumably arises from the fact that the fraction of the beam which strikes surface regions where ϕ is larger than the mean will give rise to a greater uncertainty in depth at larger depths.

For examining the effects of bulk scattering processes on depth resolution, successive layers of Al (100–300 Å) were evaporated onto the surface of a Si sample implanted with 38 keV Pb^+ ions to a dose of 5×10^{15} cm^{-2}. Low-angle RBS analysis at $\phi = 85°$ was carried out after implantation and after each subsequent evaporation. The results are summarised in fig. 7: the loss of resolution with increasing film thickness is manifested by a broadening in the measured Pb profile and an additional "tail" developing at large Al thicknesses. However, there is little change in the shape of the implanted profile initially, indicating that the loss of resolution arising from bulk scattering effects is small up to depths of $\sim$ 500 Å in Al (or, more generally, low-mass targets) for a $\phi = 85°$ backscattering geometry.

* Vibratory polished in a slurry of 0.05 μm alumina, then chemically polished with CP4.

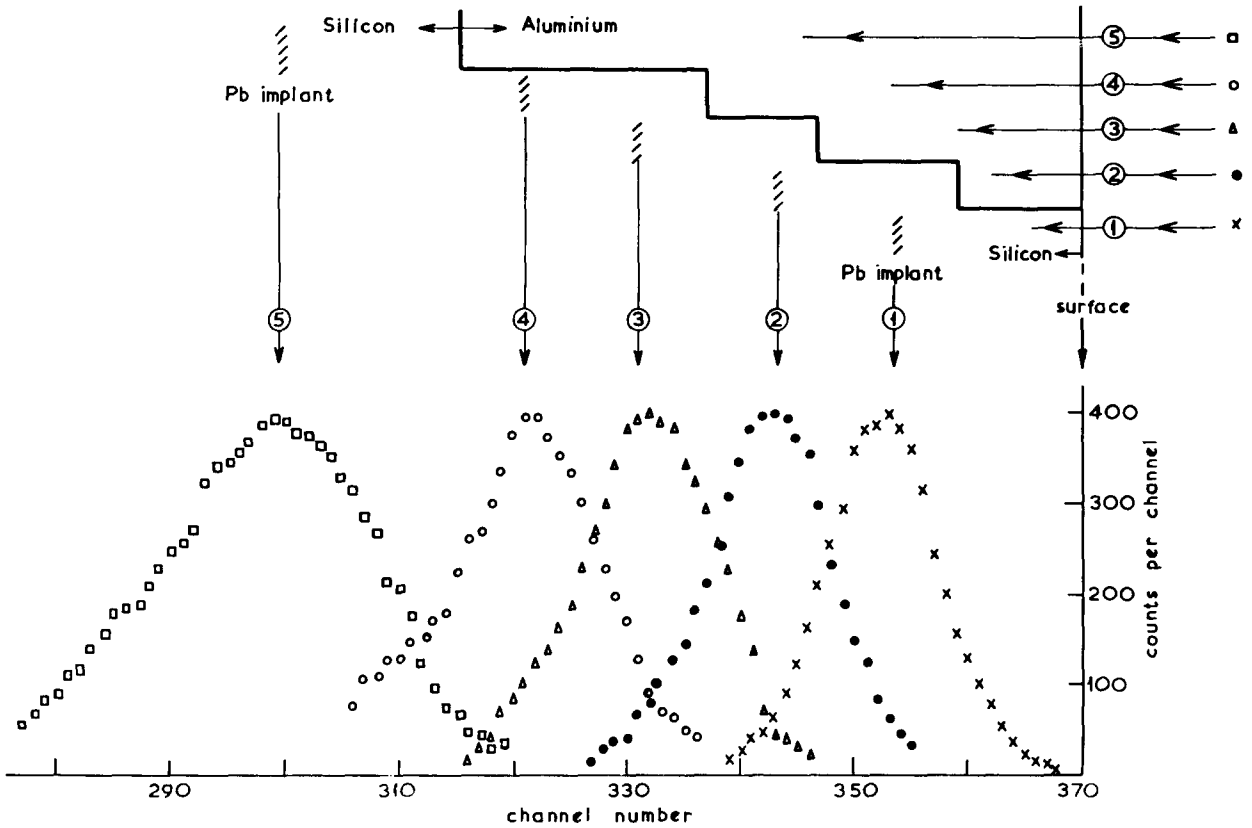

Fig. 7. 2 MeV He^+ spectra from 38 keV Pb^+ implanted into Si to a dose of 5×10^{15} cm^{-2}; (1) × is the case with no evaporated layer; (2) ● has ~120 Å of Al evaporated onto the Si surface after implantation; (3) △ has ~250 Å of Al; (4) ○ has ~370 Å; and (5) □ has ~620 Å of Al. The range R_p of 38 keV Pb in Si is about 250 Å; 5 keV/channel.

It is not possible to obtain an estimate of the absolute depth resolution of the system from either fig. 6 or 7, since the true shape of the Pb profile is not known exactly. Nevertheless, the effects of surface roughness and bulk scattering (multiple scattering and energy straggling) processes on the system resolution profile are clear: the broadening of the measured Pb profiles can only be interpreted in terms of a broadening of the resolution profile, and, moreover, the asymmetry of the Pb profile (not apparent initially) must reflect a corresponding asymmetry in the resolution profile. Thus, the shape of the low-angle depth resolution profile may depart significantly from the predominantly Gaussian resolution profile assumed with normal-incidence geometries[29]). Considerable care must be exercised when interpreting low-angle backscattering profiles exhibiting deeply penetrating tails[38,39]), since such behaviour may simply result from spurious surface topography and bulk scattering effects. Ideally, it would be desirable to measure not only the absolute depth resolution of a particular low-angle back-scattering system but the precise shape of the resolution profile.

3.4. Quantitative resolution profile measurements

The asymmetric resolution profile arising from bulk scattering and surface topography effects and the normal-incidence profile for comparison are illustrated schematically in fig. 8. These idealised profiles can be considered to arise from a single atomic layer below the target surface. The system resolution can be taken as the fwhm of the respective profiles, dz_T, as shown, and the depth of the layer below the target surface as $z_T \pm dz_R$. For near-Gaussian profiles the standard deviation ($\sim dz_T/2.4$) can be conveniently taken as a measure of the uncertainty in peak position, dz_R. To experimentally approximate an atomically thin layer, a trace amount of Au ($\sim 5 \times 10^{14}$ atoms cm^{-2}, as measured by the RBS yield) was evaporated onto the surface of the test sample. Of course, the Au atoms would probably tend to agglomerate into islands on the surface rather than form a uniform distribution[40]), but, since the total amount of Au is of the order of a monolayer, the localised Au thickness is expected to be small. Measurements of the RBS system resolution profile were then made under varying sample conditions to estimate surface topography and bulk scattering effects on the attainable depth resolution.

Fig. 9(a) shows typical experimental (Au) profiles at normal and glancing incidence: here, Si samples were first coated with a trace amount of Au, then Al evaporated to various thicknesses. The shape of the normal-incidence ($\phi = 0°$) resolution profile is not detectably altered by increasing the Al-film thickness (up to 1000 Å): the measured system energy resolution

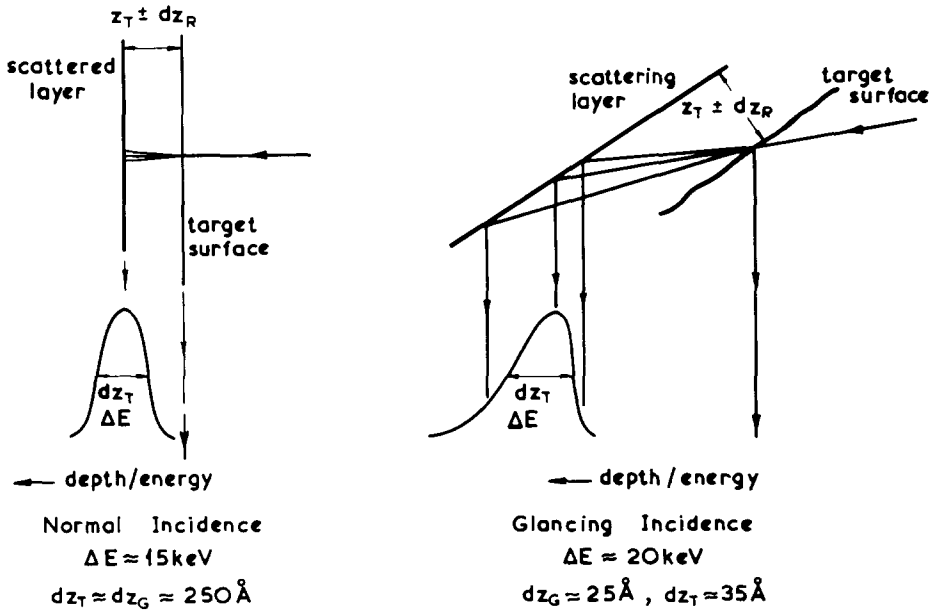

Fig. 8. A schematic showing the broader asymmetric system resolution profile which can result when $dz_L > dz_G$ for low-angle scattering geometries. The normal-incidence profile is shown for comparison. Typical energy resolutions, ΔE, and expected and measured depth resolutions (dz_G and dz_T, respectively) are indicated for both cases. See text for an explanation of other parameters.

of $\Delta E \approx 15$ keV corresponds to a depth resolution in Al of $dz_T \approx 300$ Å [from eq. (3)]. Below Al thicknesses of a few hundred Ångstroms, the $\phi = 85°$ RBS resolution profile is near-Gaussian in shape (see dotted curve) and differs from the $\phi = 0°$ profile in that the system ΔE is slightly greater (≈ 18 keV), corresponding to a depth resolution in Al of $dz_T \approx 45$ Å. For thicker Al layers, the $\phi = 85°$ system resolution profile develops a marked "tail" and broadens considerably. For example, the profile shown in fig. 9(a), where the Al thickness is ≈ 600 Å, has $\Delta E \approx 33$ keV, corresponding to a depth resolution of ≈ 85 Å.

A second method for monitoring the system depth resolution has also been employed. The approach has been to evaporate successively onto a test sample a thin Au layer followed by an Al layer (< 100 Å), and finally another thin Au layer. The RBS depth resolution can be estimated in terms of the ability to resolve the Au peaks in the Au–Al–Au "sandwich". The advantage of this method is that the improvement in depth resolution with change to low-angle geometries is more clearly visualized from the energy spectra. This is shown in fig. 9(b), where spectra for an Au–Al–Au "sandwich" (Al ≈ 65 Å) evaporated onto Si are shown: normal incidence cannot resolve the Au peaks, but $\phi = 85°$ incidence enables Au peaks to be clearly resolved, indicating that the system depth resolution in this case is somewhat better than 60 Å. The method is limited in that it is extremely difficult to evaporate an Al layer of a desired thickness (± 10 Å), and also that uniformity of the Al layer (and for that matter the thin Au layers) can never be guaranteed. In general, non-uniformity of the evaporated films will mean that the measured system depth resolution can, at the very worst, be taken as an upper limit of the actual system resolution.

Both methods described above were used to estimate the depth resolution of the $\phi = 85°$ RBS system for (1) Si samples with different surface preparation, and (2) samples subsequently evaporated with surface layers of Al, Ge, and Au to check the effects of bulk scattering processes. The results are summarised in table 2 (surface effects) and fig. 10 (bulk effects). In table 2 the measured resolution dz_T is compared with that expected from eq. (3), dz_G, using a detector energy resolution of 15 keV (fwhm). The values in brackets, dz_R, are the standard deviations of each respective profile (or

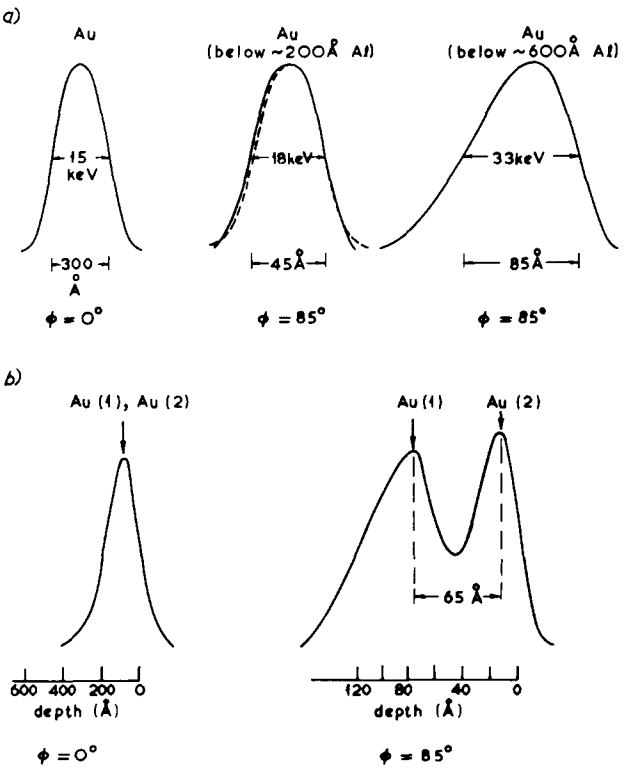

Fig. 9. Two methods used for experimentally estimating the system depth resolution: (a) a trace evaporation of Au onto the target; Au spectra are shown for normal incidence ($\phi = 0°$), and for $\phi = 85°$, with two thicknesses of Al subsequently evaporated onto the target surface. Note the "tail" (arrowed) on the $\phi = 85°$ profile with the thick Al layer; (b) An Au–Al–Au "sandwich" evaporated onto the target; $\phi = 0°$ and $\phi = 85°$ Au spectra for an Al layer of ~65 Å thickness. Note the clearly resolved Au peaks with the $\phi = 85°$ geometry.

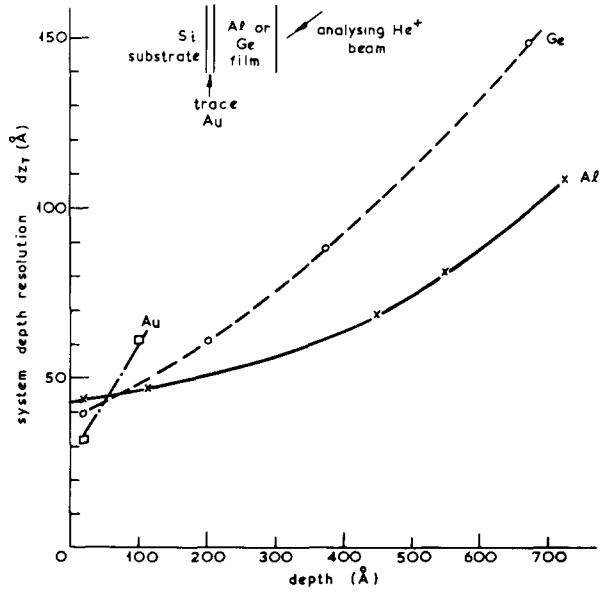

Fig. 10. A plot of the measured system depth resolution, dz_T, as a function of depth for Al, Ge, and Au targets, showing the loss of resolution arising from dz_B contributions.

TABLE 2

Measured depth resolutions, dz_T, using a $\phi = 85°$ geometry for Si samples of different surface preparation. Samples were vibratory polished in a slurry of 0.3 μm Al_2O_3, and chemically polished in CP4 for about 1½ minutes. The initial sample* was precision mechanically and chemically polished by Dow Corning Co. The expected system depth resolution, dz_G, for a 15 keV detector energy resolution is ~46 Å at $\phi = 85°$ [eq. (3)]. The term in brackets (dz_R) is the standard deviation, or equivalent, of the respective profiles.

Si surface preparation	Measured resolution dz_T (Å)	(dz_R) (Å)	Scale of dz_S	Profile shape
Commercially prepared*	52	(21)	$dz_S \ll dz_G$	near Gaussian
Vibratory polished/chem. polished	52	(21)	$dz_S \ll dz_G$	near Gaussian
5 μm Di/chem. polished	53	(21)	$dz_S \ll dz_G$	near Gaussian
Sawn/chemically polished	77	(32)	$dz_S \sim dz_G$	asymmetric
Vib. polished/*no* etch	~85		$dz_S \gtrsim dz_G$	slightly asymmetric
5 μm Di/*no* etch	~90		$dz_S > dz_G$	asymmetric

equivalent value taken from the measured profiles as $\sim dz_T/2.4$). In general, samples which were lapped and then chemically polished gave measured resolution profiles near to those expected ($dz_T \approx dz_G$), indicating that dz_S is much less than dz_G for such samples. On the other hand, the two samples which were lapped but not etched exhibited a broader asymmetric profile with $dz_S > dz_G$. All the lapped samples (both etched and non-etched) gave a surface-reflected laser beam with a divergence less than 0.1°, which can be taken as an indication of no significant long-range surface-flatness effects. However, the remaining sample which was not lapped, simply etched from a sawn surface, introduced a 2° divergence into the reflected laser beam. For this sample, the "scale" of the long-range surface flatness is therefore known, and hence the loss of resolution can be estimated from eq. (3). The estimated value was in good agreement with the measured system resolution, listed in table 2.

We can conclude from our preliminary results in table 2, that carefully lapped and etched Si samples introduce only small dz_S contributions to the overall system resolution, enabling the expected resolution dz_G to be very nearly attainable in practice. The loss of resolution with samples not chemically polished can be attributed to short-range surface-roughness effects.

In fig. 10 the measured system depth resolution has been plotted as a function of evaporated layer thickness. The observed loss of resolution with depth can be taken as an estimate of the increase in the dz_B term with depth. For depths up to ~ 500 Å in Al and ~ 300 Å in Ge the measured resolution profile remains near-Gaussian in shape with $dz_B < dz_G$; thereafter, a "tail" develops on the profile as the dz_B contribution continues to increase. As might be expected, the magnitude of the dz_B term increases with the atomic number of the evaporated layer. With the Al and Ge films, the presence of a small oxide component was observed from an "oxygen" peak in the spectra. However, since the heavier Al or Ge atoms would be the major contributors to single/multiple scattering processes of the probe beam, the presence of the oxide should have little effect on the measured resolutions. Of course, non-uniformity of the evaporated films will tend to cause the measured resolution to be somewhat greater than the actual system resolution. The limited data for Au in fig. 10 were obtained by employing a trace Ge evaporation for the resolution profile, instead of the Au used with the Al and Ge data.

4. Conclusions

It has been demonstrated that glancing-angle RBS is a successful and convenient method of improving depth resolution in the analysis of the near-surface region of solids. In principle, the technique is capable of an ultimate depth resolution approaching 20 Å in favourable circumstances – almost an order-of-magnitude improvement in resolution when compared with the usual normal-incidence RBS geometry. The prime advantage of this technique over other very high-energy-resolution arrangements is that the overall simplicity and directness of RBS analysis is preserved.

There are certain practical limitations to the attainable resolution, which must be evaluated in order to determine the absolute experimental resolution. It has been shown experimentally that surface topography effects and bulk scattering processes can result in a system resolution profile which is decidedly asymmetric: extreme care must be exercised in the interpretation of data where such effects are suspected. In some cases (particularly with samples having surface

irregularities and for analyses at large depths) these limitations can seriously degrade the expected geometrical enhancement in resolution. Nevertheless, by using carefully lapped and etched samples, our preliminary findings indicate that the expected geometrical resolution enhancement can very nearly be attained in practice by confining the analysis to the near-surface region.

Recently, glancing-angle RBS has been successfully used at the University of Salford in several studies of surface behaviour. The improved resolution has been used to monitor the stoichiometry of thin films (< 500 Å) [41]), especially for detecting composition changes close to solid interfaces and surfaces. Ion ranges[38]), ion-range profiles[39]) and high dose ion-collection characteristics[42]) are implantation parameters which have all been successfully measured. The diffusion and subsequent build-up of implant species at solid interfaces and surfaces, and the use of channelling at glancing angle are further areas which have been fruitfully investigated[20]). A more comprehensive presentation of these recent applications of glancing-angle RBS will be published elsewhere[43]).

To conclude, glancing-angle RBS has much to offer as a complementary research "tool" to supplement other standard "surface" techniques. It is envisaged that combined low-angle RBS and TEM studies of para-surface behaviour will be a powerful and rewarding method of investigating ion-implantation properties, particularly in metals where ion implantation is finding exciting materials science applications.

The author is indebted to all members of the Atomic Collisions in Solids Group at the University of Salford for their encouragement and willingness for discussion during the course of this work. Fruitful discussion with P. M. Hemenger, J. A. Davies and J. C. Kelly is also acknowledged. G. Carter, W. A. Grant and J. L. Whitton are especially to be thanked for their advice and critical reading of this manuscript.

References

1) Proc. Conf. on *Ion beam surface layer analysis* (Yorktown Heights, 1973) Thin Solid Films **19** (1973).
2) Proc. Conf. on *Application of ion beams to metals* (Albuquerque, 1973) (Plenum Press, New York, 1974).
3) W. K. Chu, J. W. Mayer, M. A. Nicolet, G. Amsel, T. Buck, and F. H. Eisen, Thin Solid Films **17** (1973) 1.
4) D. V. Morgan and E. Bøgh, Surface Sci. **32** (1972) 278.
5) W. J. De Bonte, J. M. Poate, C. M. Melliar-Smith and P. A. Levesque, ref. 2, p. 147.
6) S. U. Campisano, G. Foti, F. Grasso and E. Rimini, Proc. 6th Intern. *Vacuum* Congress (Kyoto, 1974) Jap. J. Appl. Phys. Suppl. 2 (1974) 637.
7) E. Arminen, A. Fontell and V. K. Lindroos, Phys. Status Solidi (a) **4** (1971) 663.
8) W. K. Chu, B. L. Crowder, J. W. Mayer and J. F. Ziegler, Appl. Phys. Letters **22** (1973) 490.
9) J. A. Davies, J. Denhartog, L. Eriksson and J. W. Mayer, Can. J. Phys. **45** (1967) 4053.
10) J. W. Mayer, L. Eriksson, S. T. Picraux and J. A. Davies, Can. J. Phys. **46** (1968) 663.
11) G. Dearnaley, Ann. Rev. Nucl. Sci. **4** (1974) 93.
12) R. S. Nelson, Vacuum **23** (1973) 79.
13) V. Ashworth, D. Baxter, W. A. Grant, R. P. M. Proctor and T. C. Wellington, Proc. Intern. Conf. on *Ion implantation in semiconductors and other materials* (Osaka, 1974) (Plenum press, New York, 1975).
14) D. Philips and J. P. S. Pringle, J. Electrochem. Soc. **120** (1973) 1067.
15) R. S. Blewer, Appl. Phys. Letters **23** (1973) 593.
16) W. K. Chu, E. Lugujjo, J. W. Mayer and T. W. Sigmon, ref. 1, p. 329.
17) G. Amsel, J. P. Nadai, E. d'Artemare, D. David, E. Girard and J. Moulin, Nucl. Instr. and Meth. **92** (1971) 481.
18) G. J. Thomas and S. T. Picraux, ref. 2, p. 257.
19) L. T. Chadderton and J. L. Whitton, Radiation Effects **23** (1975) 63.
20) G. A. Stephens, E. Robinson and J. S. Williams, Proc. Intern. Conf. on *Ion implantation in semiconductors and other materials* (Kyoto, 1974) to be published.
21) S. Rubin, in *Treatise on analytical chemistry* (Eds. K. Kolthoff and G. Elving; Interscience Publ., New York, 1959) pt. I, vol. IV.
22) E. Bøgh, Radiation Effects **12** (1972) 13.
23) W. F. Van der Weg, H. E. Roosendaal and W. H. Kool, Radiation Effects **17** (1973) 91.
24) I. V. Mitchell, M. Kamoshida and J. W. Mayer, J. Appl. Phys. **42** (1972) 4378.
25) L. C. Feldman, J. M. Poate, F. Ermanis and B. Schwartz, ref. 1, p. 81.
26) P. P. Pronko and J. G. Pronko, Phys. Rev. **39** (1974) 2870.
27) A. Turos, L. Wieluński and A. Barcz, Nucl. Instr. and Meth. **111** (1973) 605.
28) J. S. Williams, Radiation Effects **22** (1974) 211.
29) J. F. Ziegler and J. E. E. Baglin, J. Appl. Phys. **42** (1971) 2031.
30) J. F. Ziegler, G. W. Cole and J. E. E. Baglin, J. Appl. Phys. **43** (1972) 3809.
31) K. B. Winterbon, P. Sigmund and J. B. Sanders, Kgl. Danske Videnskab. Selskab, Mat.-Fys. Medd. **37** (1972) 14.
32) P. Sigmund and K. B. Winterbon, Nucl. Instr. and Meth. **119** (1974) 541.
33) A. D. Marwick and P. Sigmund, to be published.
34) P. B. Price, M. J. Hollis and C. S. Newton, Nucl. Instr. and Meth. **108** (1973) 605.
35) J. Lindhard, M. Scharff and H. Schiøtt, Kgl. Danske Videnskab. Selskab, Mat.-Fys. Medd. **13** (1963) 14.
36) W. S. Johnson and J. F. Gibbons, Stanford University Bookstore (1969).
37) D. Powers and W. Whaling, Phys. Rev. **126** (1962) 61.
38) J. S. Williams and W. A. Grant, Radiation Effects **24** (1975).
39) D. Fuller, J. S. Colligon and J. S. Williams, subm. to Surface Sci. (1975).
40) Au layers $\gtrsim 150$ Å tend to agglomerate into islands; see for example, E. Rimini, E. Lugujjo and J. W. Mayer, Phys. Rev. **B6** (1972) 718.
41) P. M. Hemenger and J. S. Williams, to be published.
42) J. S. Williams, Phys. Letters **51A** (1975) 85.
43) J. S. Williams, to be published.